Journal of Information Systems Engineering and Management
2025, 10(4)
e-ISSN: 2468-4376
https://www.jisem-journal.com/

Research Article

Control and Power Management of a Grid-Connected PV-FC Distributed Generation System Using PSO-Optimized Discrete-Time Integral Sliding Mode Control

Abdelkader Khoudiri[1], Mohamed Boudiaf [1]

[1] *Renewable Energy Systems Applications Laboratory (LASER), University of Djelfa, PO, Box 3117, 17000 Djelfa, Algeria*

ARTICLE INFO

Received: 15 Nov 2024

Revised: 26 Dec 2024

Accepted: 10 Jan 2025

ABSTRACT

This paper presents a control strategy for a PV-FC hybrid generation system using a three-level NPC converter based on discrete-time integral sliding mode control (DISMC) combined with particle swarm optimization (PSO). First, comprehensive modeling of the main system components is presented. Then, the design of the proposed control is detailed, followed by the optimization procedure using PSO to determine the optimal DISMC gains. A power management strategy is integrated within the control system to maximize the performance of the hybrid system, enabling decoupled control of active and reactive power in two distinct operating modes: Feeder-Flow Control (FFC) and Unit-Power Control (UPC). The approach is validated using MATLAB/Simulink simulations. Results, compared to the non-optimized DISMC, demonstrate the effectiveness and robustness of the proposed strategy.

Keywords: Discrete-time integral sliding mode control, particle swarm Optimization , PV-FC, three-level NPC inverter, power management, Feeder-Flow Control , Unit-Power Control

INTRODUCTION

The rapid growth in global energy demand and environmental issues linked to fossil fuels have made renewable energy sources the most viable alternative to large centralized fossil-fuelled power plants. Recently, distributed energy sources such as photovoltaic (PV) cells, fuel cells (FC), wind turbines, and their combinations have been increasingly used to provide a more continuous, clean, and reliable supply of electricity [1,2].

In this context, PV power systems are quiet and require less maintenance than other renewable sources. However, because solar irradiation is intermittent, a backup storage device or an additional source is necessary, especially in isolated applications [1,3]. Fuel cells, such as Solid Oxide Fuel Cells (SOFC), are highly efficient alternatives that can continuously generate DC power as long as fuel is available, achieving around 60% efficiency—higher than conventional batteries [4]. Adjusting the output power of the hybrid source increases the system's reliability and flexibility [5,6].

When operating in grid-connected mode, the hybrid source is linked to the main grid at the Point of Common Coupling (PCC) and delivers power through a DC-AC inverter. As load demand fluctuates, the system must properly regulate the power supplied by both the hybrid source and the grid to meet demand [7].

Journal of Information Systems Engineering and Management
2025, 10(4)
e-ISSN: 2468-4376
https://www.jisem-journal.com/

Research Article

Typically, the PV-FC hybrid source operates in two control modes: Unit-Power Control (UPC) and Feeder-Flow Control (FFC) [6]. In the FFC mode, the generated power by the system is variable according to the local load; if there is an extra demand, the hybrid source will handle this demand to its best and raise its generated power without the need for the grid (if possible). In the Unified Power Converter (UPC) mode, the output power of the hybrid system is regulated to maintain independence from the load demand, and it is adjusted to prioritize the needs of the primary grid. In both modes, the fuel cell serves as a secondary source, ensuring stable power delivery. The system is connected to the utility via boost DC-DC converters and a three-phase, three-level NPC inverter.

On the other hand, Nonlinear sliding mode control is known for its natural robustness; the selection of the gain offers more flexibility in the design; however, this task is time-consuming, and the best response result is not always guaranteed [10]. In addition, in digital implementation, a continuous-time sliding controller is applied only at discrete intervals, which produces a non-ideal sliding regime and can increase chattering amplitude. Adequate discrete-time formulation of sliding mode control can reduce this phenomenon and simplify the implementation procedure[11].

The main objective of this paper is to propose a fixed-frequency discrete-time integral sliding mode control optimized with the PSO algorithm (PSO-DISMC) for a three-level neutral-point clamped voltage source inverter in a grid-connected PV-FC system to ensure reliable power sharing and effective operation in both control modes. The paper is structured as follows: Section Two describes the system configuration and component modeling. Section Three presents the design and stability analysis of the proposed controller. Section Four discusses the enhancement of the controller using PSO. Section Five explains the chosen power management strategies. Finally, Section Six presents simulation results for the PV-FC grid system under the proposed control technique.

System description and modeling

The schematic of the studied PV-FC hybrid generation system and its control is shown in Figure 1. In this system, The distributed generation unit is connected to the utility grid through two DC-DC boost converters, a three-level neutral-point clamped voltage source inverter (NPC-VSI), and a series line inductor for harmonic reduction. A variable load is present on the AC side. The proposed control system uses measurements from the PV array, the load, and the grid to:

- Calculate the SOFC power reference
- Control the NPC inverter current using the PSO-DISMC method, which supplies the necessary voltages to match the reference power via SVPWM.

The reference power is set based on system measurements and the selected control mode.

Journal of Information Systems Engineering and Management
2025, 10(4)
e-ISSN: 2468-4376
https://www.jisem-journal.com/

Research Article

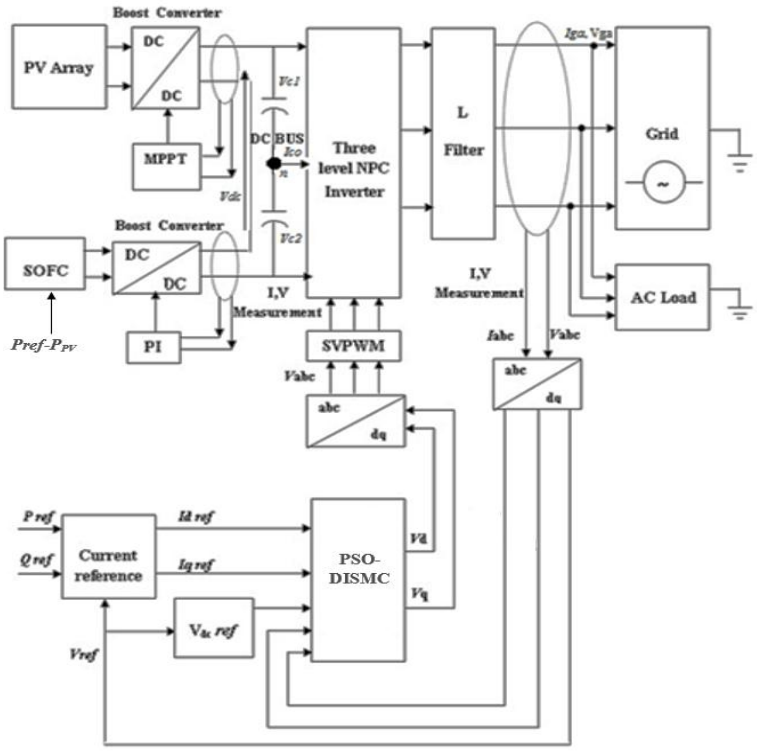

Figure 1. Structure of grid-connected PV-FC with the proposed control of the NPC inverter

Photovoltaic Array (PV)

The photovoltaic array is the main source of the hybrid system. In the single-diode equivalent circuit, the mathematical relationship between current and voltage can be expressed as follows[12]:

$$I = N_P I_{ph} - N_P . I_s . \left[exp\left(\frac{q}{A.K.T} \left(\frac{V}{N_S} + \frac{I.R_S}{N_P} \right) \right) - 1 \right] - \frac{N_P}{R_{sh}} \left(\frac{V}{N_S} + \frac{I.R_S}{N_P} \right) \quad (1)$$

$$I_{ph} = \left(\frac{S}{S_{ref}} \right) . \left[I_{ph,ref} + C_T \left(T - T_{ref} \right) \right] \quad (2)$$

$$I_S = I_{S,ref} . \left(\frac{T}{T_{ref}} \right)^3 . exp\left[\frac{q.E_g}{A.K} . \left(\frac{1}{T_{ref}} - \frac{1}{T} \right) \right] \quad (3)$$

Where: I_{ph} is the photocurrent; I_S: is the diode saturation current.

N.B: Parameters definitions, values, and units are provided in the Appendix.

Journal of Information Systems Engineering and Management
2025, 10(4)
e-ISSN: 2468-4376
https://www.jisem-journal.com/

Research Article

Solid Oxide Fuel Cell (SOFC)

Solid oxide fuel cells (SOFC) are a promising alternative to traditional renewable sources and other fuel cell technologies, thanks to their high efficiency, low environmental impact, and high reliability. A key advantage of SOFCs is their ability to operate at high temperatures, making them suitable for both small and large-scale stationary power generation. To model the SOFC, the following assumptions are considered [13]:

- Nernst's equation is applicable.
- The fuel cell temperature is constant and gases are ideal.

The dynamics of the SOFC are described by the following equations[9]:

$$P_{ref} = V_{fc}.I_{ref} \quad (4)$$

$$V_{fc} = N_0.\left[E_0 + \frac{RT}{2F}\ln\left(\frac{P_{H2}PO_2^{0.5}}{PH_2O}\right)\right] - rI_{fc} \quad (5)$$

$$\frac{dI_{fc}}{dt} = \frac{1}{T_e}\left[-I_{fc} + I_{ref}\right] \quad (6)$$

$$\frac{dq_{H2}^{in}}{dt} = \frac{1}{T_f}\left[-q_{H2}^{in} + \frac{2K_r}{U_{opt}}I_{fc}\right] \quad (7)$$

$$\frac{dP_{H2}}{dt} = \frac{1}{\tau_{H2}}\left[-P_{H2} + \frac{1}{K_{H2}}\left[q_{H2}^{in} - 2K_rI_{fc}\right]\right] \quad (8)$$

$$\frac{dP_{O2}}{dt} = \frac{1}{\tau_{O2}}\left[-P_{O2} + \frac{1}{K_{O2}}\left[\frac{1}{r_{HO}}q_{H2}^{in} - 2K_rI_{fc}\right]\right] \quad (9)$$

$$\frac{dP_{H_2O}}{dt} = \frac{1}{\tau_{H_2O}}\left[-P_{H_2O} + \frac{2K_r}{K_{H_2O}}I_{fc}\right] \quad (10)$$

Where: P_{ref} Reference power (Kw), V_{fc} Operating DC voltage (V), I_{fc}: stack current (A)

N.B: Parameters definitions and their values and units are given in the Appendix

Journal of Information Systems Engineering and Management
2025, 10(4)
e-ISSN: 2468-4376
https://www.jisem-journal.com/

Research Article

DC-DC Converter

The studied PV-FC hybrid system includes two DC-DC boost converters that interface the PV and SOFC sources to the DC bus. An average model is used for analysis [14]. For the PV source, the incremental conductance (INC-MPPT) algorithm is applied to extract maximum power [15]. For the SOFC source, the boost converter regulates the required fixed DC voltage using a classic PI controller, with each converter controlled according to its source specifications.

Grid-connected three-level NPC voltage source inverter

The inverter is a key component for the successful operation of the hybrid PV-FC power system. Multilevel inverters are especially attractive for medium and high voltage applications, as they can reduce high-order harmonics introduced by PWM modulation at the same switching

frequency, which in turn reduces the size of the required output filter [16]. The model of the three-level NPC-VSI is developed under the following assumptions:

- The AC voltage is a balanced three-phase system.
- The power switches are ideal.
- All circuit elements are linear and time-invariant (LTI) [17].

On the AC side, its mathematical model is given by [18,19]:

$$\frac{d}{dt}\begin{bmatrix} i_a \\ i_b \\ i_c \end{bmatrix} = \begin{bmatrix} \frac{-R}{L} & 0 & 0 \\ 0 & \frac{-R}{L} & 0 \\ 0 & 0 & \frac{-R}{L} \end{bmatrix} \begin{bmatrix} i_a \\ i_b \\ i_c \end{bmatrix} - \frac{1}{L}\begin{bmatrix} V_{ga} - e_a \\ V_{gb} - e_b \\ V_{gc} - e_c \end{bmatrix} \quad (11)$$

Where: e_i (i= a, b, c) , V_{gi} (i= a, b, c) are respectively the inverter voltage and the primary grid AC voltage, and, L, R are the output filter and its internal resistance.

On The DC side, the input voltages and currents of the two capacitors are:

V_{C1}, V_{C2} and: I_{C1}, I_{C2} :

$I_{C0} = I_{C1} + I_{C2}$ and $\frac{d}{dt}\begin{bmatrix} V_{C1} \\ V_{C2} \end{bmatrix} = \frac{d}{dt}\begin{bmatrix} I_{C1} \\ I_{C2} \end{bmatrix}$

In a balanced condition, one can put: $V_{C1} = V_{C2} = V_C$; $I_{C1} = I_{C2} = I_C$

In addition, the output AC active and reactive powers of the inverter are:

$$P_g = V_{ga} i_{ga} + V_{gb} i_{gb} + V_{gc} i_{gc} \quad (12)$$

Journal of Information Systems Engineering and Management
2025, 10(4)
e-ISSN: 2468-4376
https://www.jisem-journal.com/

Research Article

$$Q_g = \frac{1}{\sqrt{3}}\left(V_{gab}i_{gc} + V_{gbc}i_{ga} + V_{gca}i_{gb}\right) \quad (13)$$

Where: $V_{gi}(i=a, b, c)$ and V_{gab} , V_{gbc} ,V_{gca} are respectively the phase-neutral and phase-to-phase voltages of the AC bus, and, i_{ga} , i_{gb} , i_{gc}: are the three-phase currents injected into the AC grid.

In the (d, q) frame, the state space model of the NPC inverter has the form[17,18]:

$$\dot{X}(t) = AX(t) + BU(t) + C \quad (14)$$

With: $X(t) = \left[i_d, i_q, V_{dc}\right]^T$, $U(t) = \left[V_d, V_q, I_{dc}\right]^T$

$$A = \begin{bmatrix} \frac{-R}{L} & \omega & 0 \\ -\omega & \frac{-R}{L} & 0 \\ 0 & 0 & 0 \end{bmatrix}, B = \begin{bmatrix} \frac{1}{L} & 0 & 0 \\ 0 & \frac{1}{L} & 0 \\ 0 & 0 & \frac{1}{C_{eq}} \end{bmatrix}, C = \begin{bmatrix} \frac{-1}{L}V_{gd} \\ \frac{-1}{L}V_{gq} \\ 0 \end{bmatrix}$$

And,(V_{gd} ,V_{gq}) are the (d, q) axis components of the primary grid voltages, (V_d ,V_q): the converter output voltages. I_{dc} : the equivalent direct current, *and* i_d and i_q : the line currents ω is the rotation frequency calculated using phase-locked loop (*PLL*).

V_{dc} is the dynamic DC equivalent voltage described as :

$$C_{eq}\frac{dV_{dc}}{dt} = I_{dc} \quad (15)$$

With: $C_{eq} = C/2$ is the DC-link equivalent capacitor.

Subsequently, the instantaneous (d, q) active and reactive powers delivered to the grid are given by [18]:

$$P_g(t) = \frac{3}{2}\left(V_{sd}(t)i_d(t) + V_{sq}(t)i_q(t)\right) \quad (16)$$

$$Q_g(t) = \frac{3}{2}\left(-V_{sd}(t)i_q(t) + V_{sq}(t)i_d(t)\right) \quad (17)$$

the reference frame is synchronized with the grid voltage, V_{gq}= 0,V_{gd}= V_g, thus :

$$P_g(t) = \frac{3}{2}\left(V_g(t)i_d(t)\right), \quad (18)$$

$$Q_g(t) = \frac{3}{2}\left(-V_g(t)i_q(t)\right) \quad (19)$$

Journal of Information Systems Engineering and Management
2025, 10(4)
e-ISSN: 2468-4376
https://www.jisem-journal.com/

Research Article

Proposed control strategy

The proposed control strategy is based on discrete-time integral sliding mode control. This approach is chosen for its natural robustness against fluctuations and uncertainties in both DC sources and grid voltage, as well as its ability to eliminate the reaching phase. The main objective is to drive the system state to the sliding surface in finite time and ensure it remains there, using an appropriate control law so that the state trajectories follow σ = 0 with controlled and stable dynamic behavior [20,21].

First, let's consider three new variables:

$X_{e1}(t) = (i_{dref} - i_d), X_{e2}(t) = (i_{qref} - i_q)\ ,\ X_{e3}(t) = (V_{dcref} - V_{dc})$

Where: (i_{dref}, i_{qref}) reference currents ,and V_{dcref} is fixed by the system designer

The calculation of (i_{dref}, i_{qref}) is done by mean of power references (P_{ref}, Q_{ref}) assuming that the grid q-axis represents the reactive component, then:

$$I_{dref} = \frac{2\,P_{ref}}{3V_{ref}}, \qquad I_{qref} = \frac{-2\,Q_{ref}}{3V_{ref}} \tag{20}$$

Now, considering that : $X_e(t) = [X_{e1}(t)\ , X_{e2}(t)\ , X_{e3}(t)]^T$; then , the state-space error dynamics model of the system can be achieved as:

$$\dot{X_e}(t) = A_e X_e(t) + B_e U(t) + C_e \tag{21}$$

Where: $A_e = A,\ B_e = -B,\ C_e = C - A\left[i_{dref}\ , i_{qref}\ , V_{dcref}\right]^T$

The control performance of the previous system is affected by model inaccuracies, parameter disturbances, dead time, unbalanced input capacitors, high voltage harmonics, etc. It is assumed that these disturbances are a bounded lumped perturbation $d_e(t)$ [21]:

$$|d_e(t)| \leq D_M \tag{22}$$

Where : D_M denotes a known positive constant.

Then, the system in eq.(21) becomes :

$$\dot{X_e}(t) = A_e X_e(t) + B_e U(t) + D_e(t) \tag{23}$$

With: $D_e(t) = C_e + d_e(t)$

Finally, The discrete-time state-space error dynamics model of the system in eq.(23) with disturbance, will be obtained through the state transition matrix and the sampling at small time intervals T:

Journal of Information Systems Engineering and Management
2025, 10(4)
e-ISSN: 2468-4376
https://www.jisem-journal.com/

Research Article

$$X_e(k+1) = A_{ed}X_e(k) + B_{ed}U(k) + D_{ed} \quad (24)$$

Where: A_{ed}, B_{ed} and D_{ed} are discrete-time system matrices, given by :

$$A_{ed} = e^{A_eT},\ B_{ed} = \int_0^T e^{A_e\tau}B_e d\tau\ , D_{ed} = \int_0^T e^{A_e\tau}D_e(kT + (T-\tau))d\tau$$

Next, The adopted sliding manifold is chosen to have both proportional and integral actions;

In discrete time, it is given by:

$$\sigma(k) = K_P X(k) + K_i T \sum_{j=0}^{k-1} X(j)\ , k = 0,1,2 \ldots \quad (25)$$

With: K_P , K_i are the parameters matrices.

The adequate choice of (K_P , K_i) guarantees that the system is in the sliding manifold, defined by:

$$\sigma(k+1) = K_P X(k+1) + K_i T \sum_{j=0}^{k} X(j) = 0 \quad (26)$$

Therefore:

$$\sigma(k+1) = K_p(X_e(k+1) - X_e(k)) + K_i T X_e(k) + \sigma(k) \quad (27)$$

Solving the previous equation, we can verify that:

$$X_e(k+1) = (I - K_P^{-1}K_i T)X_e(k) \quad (28)$$

Eq.(28) describes the system dynamics on the switching manifold, where the system state depends only on the controller's parameter choice.

Hence, the proposed controller has the following form:

$$U(k) = U_{eq}(k) + U_{NL}(k) \quad (29)$$

With: $U_{eq}(k)$ is the discrete-time equivalent control which is obtained by replacing $U(k)$ by $U_{eq}(k)$ in the sliding manifold ($\sigma(k+1) = 0$), and $U_{NL}(k)$ is the nonlinear control.

To calculate the equivalent control $U_{eq}(k)$, consider first eq.(25) recurrence:

$$X_e(k) = A_{ed}X_e(k-1) + B_{ed}U(k-1) + D_{ed} \quad (30)$$

Then, in the eq.(27), replacing $X_e(k)$ and $X_e(k+1)$ by eq. (30) and eq.(24) , one can obtain:

$$\sigma(k+1) = \left[K_p(A_{ed} - I) + K_i T\right]\left[A_{ed}X(k-1) + B_{ed}U_{eq}(k-1) + D_{ed}\right] + K_p D_{ed} + K_p B_{ed}U_{eq}(k) + \sigma(k) \quad (31)$$

Finally, Replacing eq.(31) in eq.(26), therefore, control vector $U_{eq}(k)$ is:

Journal of Information Systems Engineering and Management
2025, 10(4)
e-ISSN: 2468-4376
https://www.jisem-journal.com/

Research Article

$$U_{eq}(k) = -\left(K_p B_{ed}\right)^{-1}\left[\left[K_p(A_{ed}-I)+K_iT\right]\left[A_{ed}X(k-1)+B_{ed}U_{eq}(k-1)+D_{ed}\right]+K_pD_{ed}+\sigma(k)\right] \quad (32)$$

Consequently, applying $U_{eq}(k)$, the state vector starting from un initial point x_o can theoretically reach the sliding manifold in one sampling time.

For practical consideration, the equivalent control is limited to:

$$U_{Min} < \left\|U_{eq}(k)\right\| < U_{Max} \quad (33)$$

with : U_{Min} , $U_{Max}$are fixed limitation values.

In addition, to reduce the reaching time and enhance the robustness of the SMC, nonlinear control $U_{NL}(k)$ must be added; In our case, the *signum* function is replaced by the *saturation* function:

$$U_{NL}(k) = -\left(K_p B_{ed}\right)^{-1} E_{ed}.sat\left(\sigma(k)\right) \quad (34)$$

Where: E_{ed} is a matrix with constant non-negative elements.

And: $sat(\sigma(k)) = \begin{cases} \frac{\sigma(k)}{U_{Min}} \text{ if } -U_{Min} \le \sigma(k) \le U_{Min} \\ sign\left(\sigma(k)\right) \text{ else} \end{cases}$

Hence, the proposed DISMC is defined by eq.(32) and eq.(34).

The obtained $(V_d(k), V_q(k))$ voltages can be, then, modulated directly using SVPWM technique, which simplifies the practical implementation of the proposed controller.

Stability Analysis of the DISMC

In the case of discrete-time systems, the Lyapunov necessary and sufficient condition assuring both sliding motion and convergence onto the sliding manifold σ is[20,22]:

$$\|\sigma(k+1)\| < \|\sigma(k)\| \quad (35)$$

From eq.(31), $\|\sigma(k+1)\|$ is:

$$\|\sigma(k+1)\| = \left\|\left[K_p(A_{ed}-I)+K_iT\right]\left[A_{ed}X(k-1)+B_{ed}U_{eq}(k-1)+D_{ed}\right]+K_pD_{ed}+K_pB_{ed}U_{eq}(k)+\sigma(k)\right\| \quad (36)$$

Using the Minkowski inequality in eq.(36):

$$\|\sigma(k+1)\| \le \left\|\left[K_p(A_{ed}-I)+K_iT\right]\left[A_{ed}X(k-1)+B_{ed}U_{eq}(k-1)+D_{ed}\right]+K_pD_{ed}\right\| + \left\|K_pB_{ed}U_{eq}(k)\right\| + \|\sigma(k)\|$$

Furthermore, using Holder's inequality, then:

$$\|\sigma(k+1)\| \le \left\|\left[K_p(A_{ed}-I)+K_iT\right]\left[A_{ed}X(k-1)+B_{ed}U_{eq}(k-1)+D_{ed}\right]+K_pD_{ed}\right\| + \left\|K_pB_d\right\|.\left\|U_{eq}(k)\right\| + \|\sigma(k)\|$$

Journal of Information Systems Engineering and Management
2025, 10(4)
e-ISSN: 2468-4376
https://www.jisem-journal.com/

Research Article

Therefore, the condition in eq.(35) is always satisfied if:

$$\left\|\left[K_p(A_{ed}-I)+K_iT\right]\left[A_{ed}X(k-1)+B_{ed}U_{eq}(k-1)+D_{ed}\right]+K_pD_{ed}\right\|+\left\|K_pB_d\right\|.\left\|U_{eq}(k)\right\|>0$$

Thus :

$$\left\|K_pB_d\right\|.\left\|U_{eq}(k)\right\| > -\left\|\left[K_p(A_{ed}-I)+K_iT\right]\left[A_{ed}X(k-1)+B_{ed}U_{eq}(k-1)+D_{ed}\right]+K_pD_{ed}\right\| \quad (37)$$

Hence, choosing:

$$\left\|K_pB_d\right\|>0 \text{ and } \left\|U_{eq}(k)\right\|>0 \quad (38)$$

which is practically verified Will satisfy stability condition in eq.(35).

Consequently, by choosing the adequate parameters (K_P , $K_i$matrices), the stability condition is verified and $\|\sigma(k+1)\|$ will decrease monotonically to 0.

Selection of the DISMC gains using PSO

To calculate the optimized controller gains , let first consider the search space : $\Phi \subset$ Rn and the objective function f: $\Phi \rightarrow \Gamma \subseteq R$, the swarm is defined as a group: $S = \{X_1, X_2, \ldots\ldots, X_N\}$

The objective is to move each particle (i) of N defined by its couple : position and velocity $(x_i(t_e), v_i(t_e))$ at each iteration (t_e) based on the objective function f [23,24].

The individual work of the particle consists of memorizing its solution (p_i), defined as :

$$p_i(t_e) = \arg min\, f_i(t_e) \quad (39)$$

To simulate collective behavior, all the individual solutions are put into memory with :

$$X_{ij}(t_e+1) = X_{ij}(t_e) + v_{ij}(t_e+1)\,, i = 1,2,\ldots,N \quad ; \quad j = 1,2,\ldots,n.$$

$$v_{ij}(t_e+1) = \omega \cdot v_{ij}(t_e) + R_P \cdot \psi_P\left(P_{ij}(t_e) - X_{ij}(t_e)\right) R_g \cdot \psi_g\left(P_{gj}(t_e) - X_{ij}(t_e)\right) \quad (40)$$

Where : R_P and R_g are random variables uniformly distributed in [0, 1].

And : ω, ψ_P , ψ_g are called inertia, cognitive, and social weighting factors, usually :

$\omega \leq 1$ and $\psi_P + \psi_g = 4$.

Next , the best general solution P_g visited by all the particles, is :

$$p_g(t_e) = \arg min\, f_i(p_i(t_e)) \quad (41)$$

and, the next iteration will be [23,24] :

Journal of Information Systems Engineering and Management
2025, 10(4)
e-ISSN: 2468-4376
https://www.jisem-journal.com/

Research Article

$$p_i(t_e+1) = \begin{cases} x_i(t_e+1) & \text{if } f\,(x_i(t_e+1)) \le p_i(t_e) \\ P_i(t_e) & \text{else} \end{cases} \quad (42)$$

Choice of the search space and the objective function

The PSO is done offline in the search space to obtain the optimal gain matrices noted (K_{PO}, K_{iO}). The chosen search space Φ is given by:

$$\Phi : K_P \in]0\ I_{pMax}] \ ; \quad K_i \in]0\ I_{iMax}] \quad (43)$$

Where: (I_{pMax}, I_{iMax}) are the gains of which $\|U_{eq}(k)\| = U_{Max}$, starting the search from the gains K_{PNO} and K_{iNO} , where, the gains K_{PNO} and K_{iNO} are obtained through the trial-error tests series (best effort).

The choice of the test duration noted T_{test} determines the number of iterations (n); Here, T_{test} is obtained using the non-optimized response (with K_{PNO} and K_{iNO})that contains both transient state and steady-state information, thus :

$$T_{test} \ge 5\tau \quad (44)$$

where: τ is the response time obtained with K_{PNO} and K_{iNO}

Next, the chosen objective function f to be minimized is the norm of the quadratic error (e_q) between the generated power by the PV-FC at the inverter and the power reference during the test time T_{test}; this choice reflects the accumulated error in the control as an indicator to judge the performance of controller, thus :

$$f = norm\,(E_q) \quad (45)$$

With: E_q is the vector that contains all the quadratic errors $e_q(t_e)$

$$\begin{cases} e_q(t_e) = (P_{ref} - P_{inv}(t_e))^2 \\ P_{inv}(t_e) = P_{PV}(t_e) + P_{SOFC}(t_e) \end{cases} \quad (46)$$

Power management

To demonstrate the effectiveness of the proposed PSO-DISMC strategy, the following power management strategy is adopted:

- Reference active and reactive powers are generated by the system using both of its two sources .
- The PV system acts as the primary source, while the SOFC operates as a secondary source to ensure smooth and reliable power delivery to the load and the grid, even during poor weather conditions or at night.
- The system operates in both Unit-Power Control (UPC) and Feeder-Flow Control (FFC) modes, depending on the local load and grid demand.

Journal of Information Systems Engineering and Management
2025, 10(4)
e-ISSN: 2468-4376
https://www.jisem-journal.com/

Research Article

- In both modes, If the local load demand is less than the reference power generated by the PV-FC system, the excess is injected into the grid. Otherwise, the grid supplies the additional power required to meet the load demand.

Simulation results are presented in the next section.

Simulation results

To validate the proposed PSO-DISMC controller, the overall grid-connected PV-FC hybrid system is simulated in MATLAB/Simulink for both operating modes. The controller and system parameters are provided in the Appendix. For comparison, the PV-FC system is re-simulated under the same conditions using both the non-optimized and the PSO-DISMC controller, with identical test durations. The objective is to demonstrate the effectiveness of the proposed controller in power management. For this purpose, a PV-SOFC system is considered :

$P_{PVMAX} = 100\ KW,\ P_{SOFCMAX} = 50\ KW$

The system components as well as the controller parameters are given in the Appendix

In addition, The following standard parameters are considered for the PSO Algorithm:

N=20, ω=0.5, $\psi_P = \psi_g$ =2 , and, Variable temperature and irradiance conditions, are considered, as shown in Fig. 2,

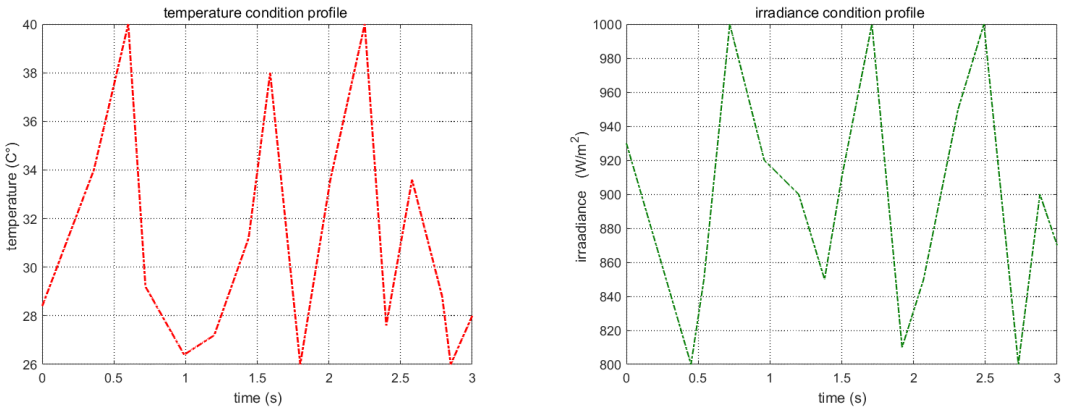

(a) (b)

Figure 2. Temperature and Irradiance conditions: (a) Temperature, (b) Irradiance

Feeder Flow Control (FFC) mode

In this case, the SOFC and PV-generated powers will vary to ensure local demand. During the test, the following local load step reference variations are supposed to be:

$$P_{load\ ref} = \begin{cases} 100\ KW & t \leq 1s \\ 150\ KW & 1 \leq 1st \leq 2s \\ 200\ KW & 2 \leq 1st \leq 3s \end{cases}, Q_{load\ ref} = 1KVar$$

The main simulation results are shown in the following figures:

Journal of Information Systems Engineering and Management
2025, 10(4)
e-ISSN: 2468-4376
https://www.jisem-journal.com/

Research Article

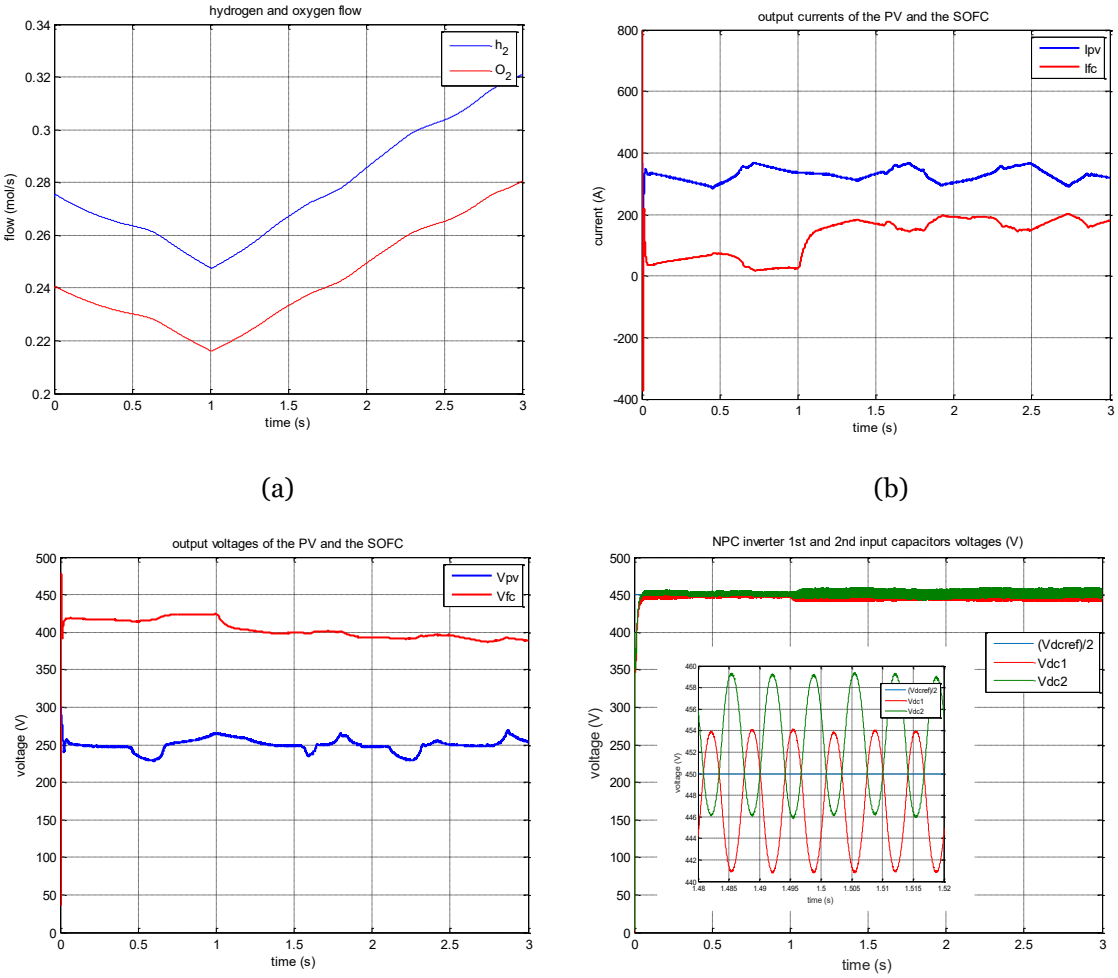

(a) (b)

(c) (d)

Figure 3. DC side results of the FFC mode under PSO-DISMC: (a) H2 and O2 input flows of the SOFC, (b) Output currents, (c) Output voltages, (d) NPC inverter input capacitors voltages.

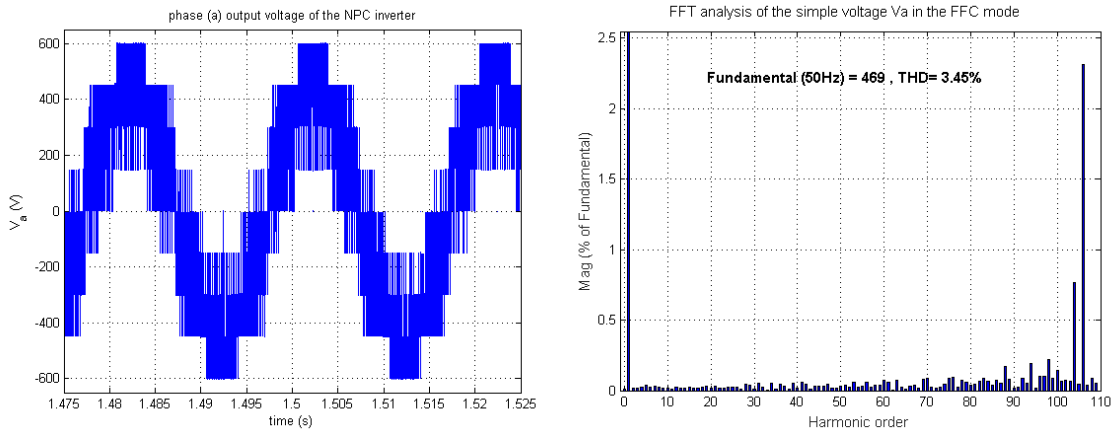

(a) (b)

Journal of Information Systems Engineering and Management
2025, 10(4)
e-ISSN: 2468-4376
https://www.jisem-journal.com/

Research Article

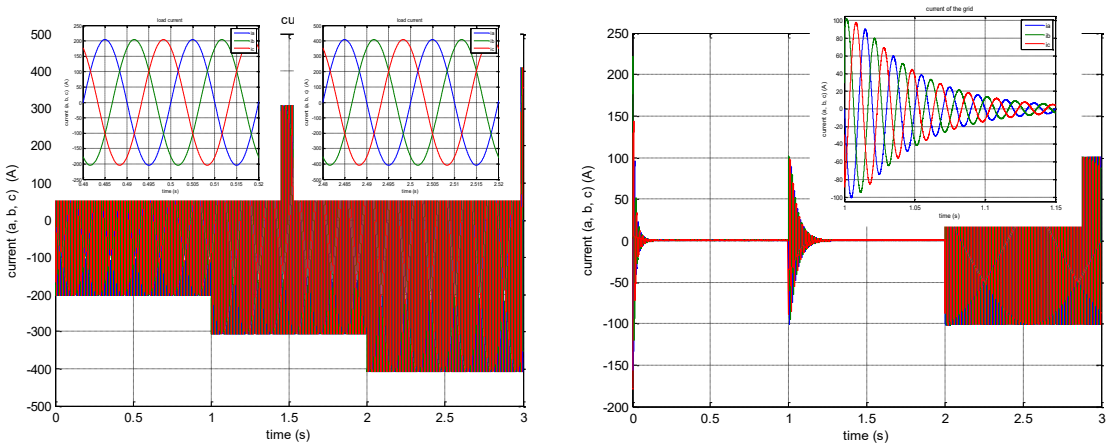

(c) (d)

Figure 4. AC side results of the FFC mode under PSO-DISMC: (a) NPC inverter output simple voltage, (b) FFT spectrum of the L filtered voltage, (c) Load currents, (d) Grid currents

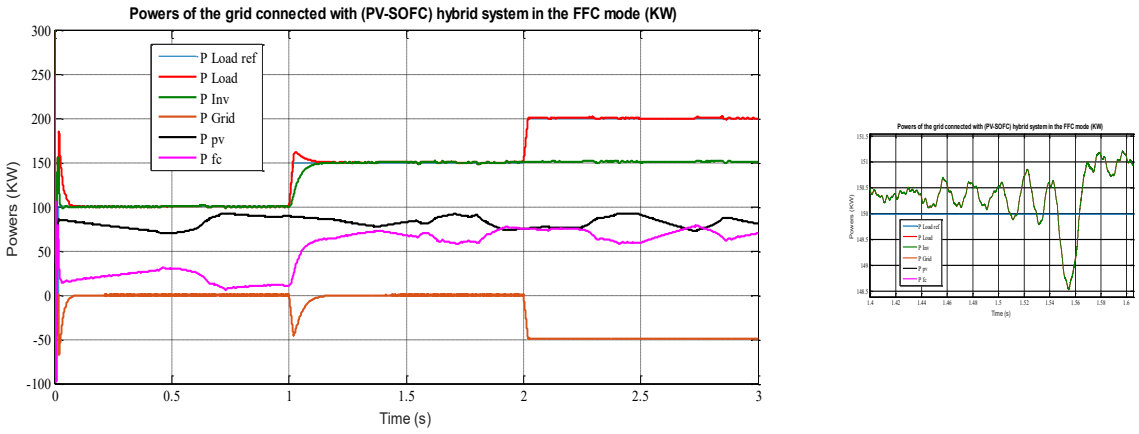

(a)

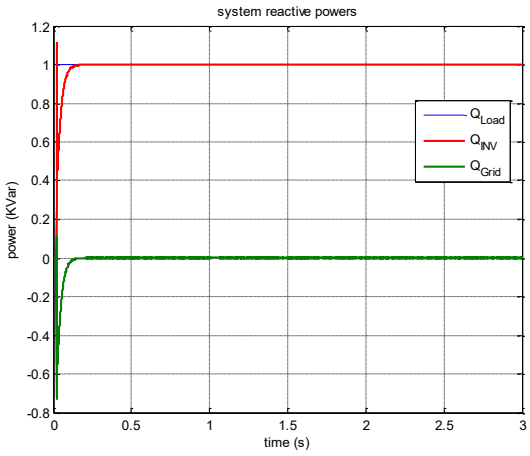

(b)

Figure 5. Grid-connected (PV-SOFC) system powers in the FFC mode under PSO-DISMC: (a) active powers (with Zoom), (b) reactive powers

Journal of Information Systems Engineering and Management
2025, 10(4)
e-ISSN: 2468-4376
https://www.jisem-journal.com/

Research Article

From Fig. 3.a, the initial value of the hydrogen flow qH2 is 0.274 (mol/s), . This value matches the theoretical value in the SOFC model when the initial current is set to 100 A. The oxygen flow is obtained by dividing the hydrogen flow by the hydrogen-to-oxygen ratio. In the model, this ratio is set to 1.145, so the initial oxygen flow rate is 0.239 mol/s.

The output power of the SOFC (see Fig. 3.b and Fig. 3.c) depends on the PV output power. Under unfavorable atmospheric conditions, both the voltage and current of the SOFC increase. This compensates for the drop in PV power and ensures the power objective is met according to the load (see t<1s t<2s in Fig. 5.a). If both the PV and SOFC reach their maximum output, the system maintains its production level, and the grid supplies any remaining power needed by the load (t=1s and t>2s in Fig. 5.a). Decoupled control of reactive power is also achieved, and the hybrid system meets the load requirement $Q_{load\,ref} = 1\ KVar$ (Fig. 5.b).

Throughout the loading conditions, the two input capacitors of the NPC inverter remain close to 450 V (Fig. 3.d). This is accomplished by using PI and INC-MPPT controls for the boost converters.

With PSO-DISMC, the PV-FC system meets the load requirements through the three-level NPC inverter (Fig. 4.a). The controller uses current information to generate and adjust the reference control voltages in the (d, q) frame at each time step. These voltages are modulated using SVPWM, resulting in a three-level output voltage with low THD (3.45%) and balanced currents (Fig. 4.c and Fig. 4.d). The proposed strategy is robust against DC input voltage fluctuations, weather changes, and local AC load variations.

Unit-power control (UPC) mode

In this mode, the required *grid* active power is *prioritized* as a reference; for this, the following step variations are supposed :

$P_{grid\,ref} = 50\ KW \quad , Q_{grid\,ref} = 1KVar$

However, a local load is considered as follows:

$$P_{load} = \begin{cases} 100\ KW & t \leq 1s \\ 150\ KW & t > 2s \end{cases} , Q_{load} = 0$$

The PV-FC system operates under the same weather conditions (Fig. 2).

The following figures give the main obtained results:

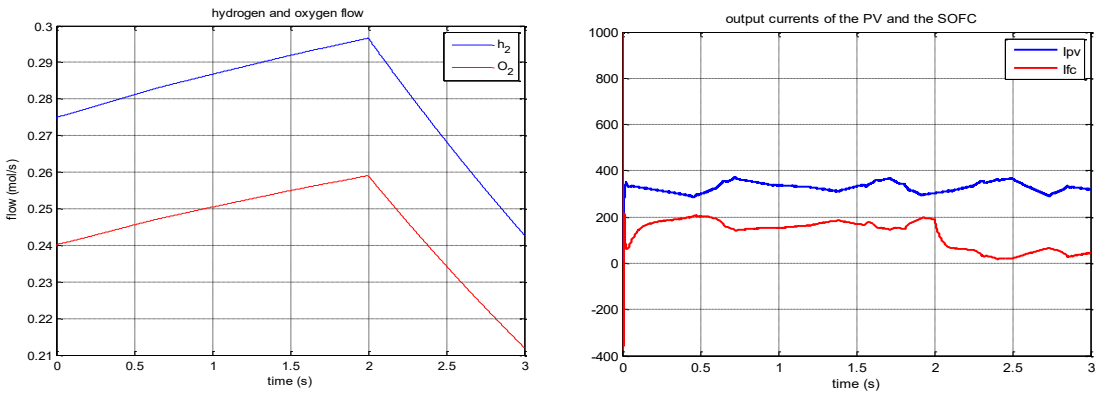

(a) (b)

Journal of Information Systems Engineering and Management
2025, 10(4)
e-ISSN: 2468-4376
https://www.jisem-journal.com/

Research Article

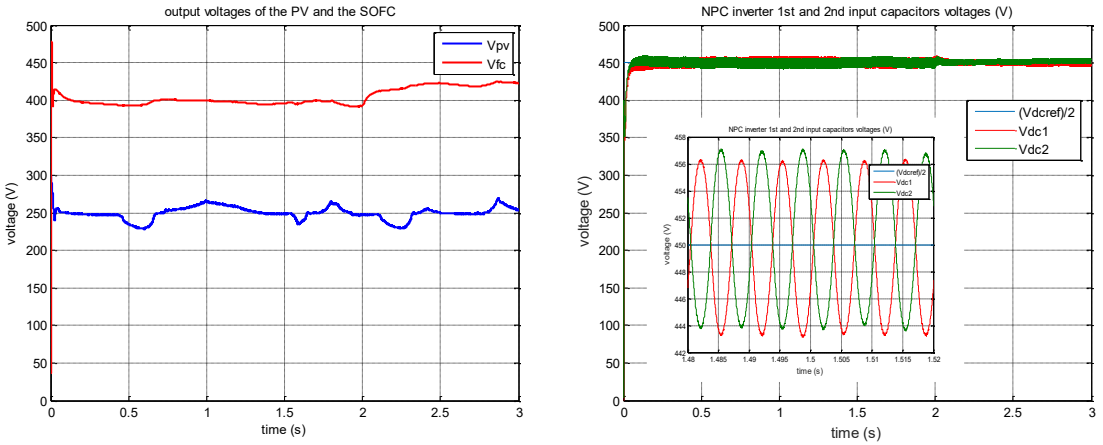

(c) (d)

Figure 6. DC side results of the UPC mode under PSO-DISMC: (a) H2and O2 input flows of the SOFC, (b) Output currents, (c) Output voltages, (d) NPC inverter input capacitors voltages.

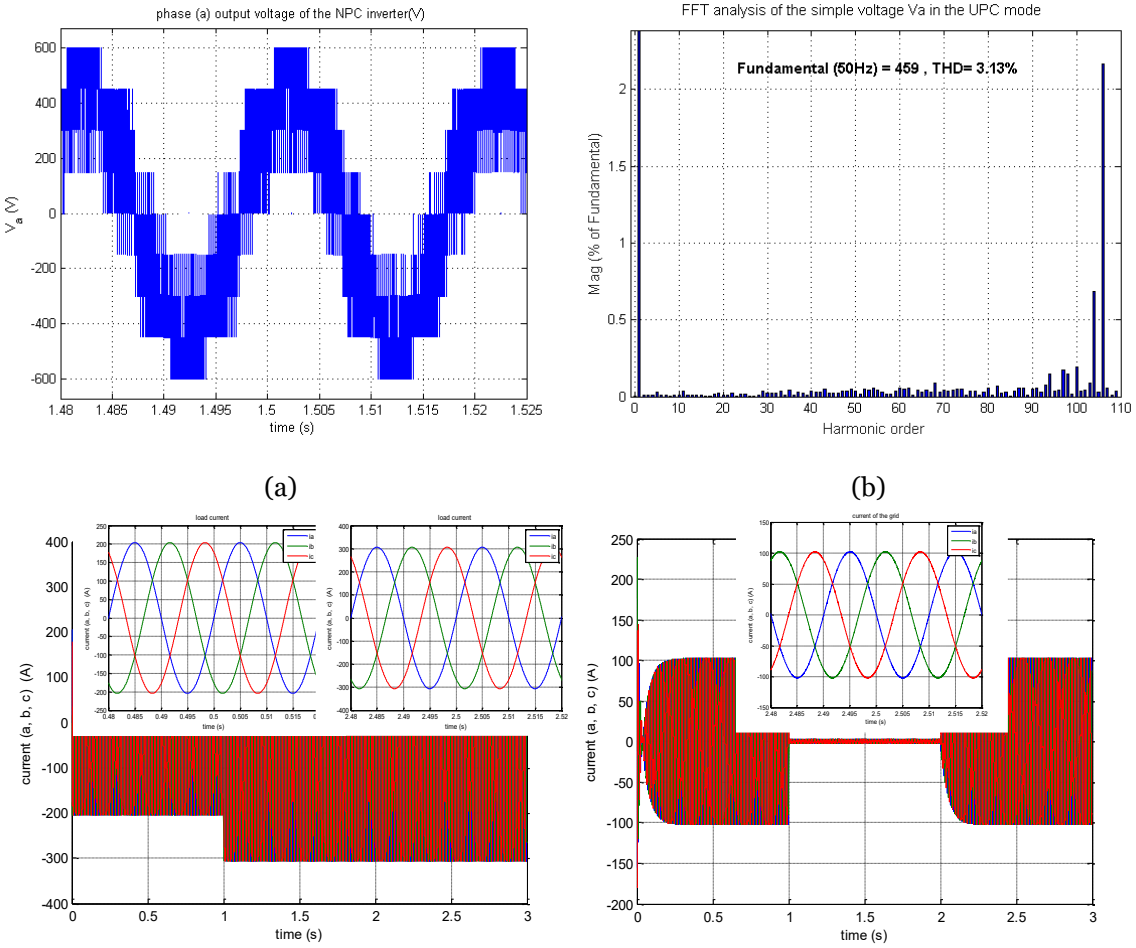

(a) (b)

(c) (d)

Figure 7. AC side results of the UPC mode under PSO-DISMC: (a) NPC inverter output simple voltage, (b) FFT spectrum of the L filtered voltage, (c) Load currents, (d) Grid currents

Journal of Information Systems Engineering and Management
2025, 10(4)
e-ISSN: 2468-4376
https://www.jisem-journal.com/

Research Article

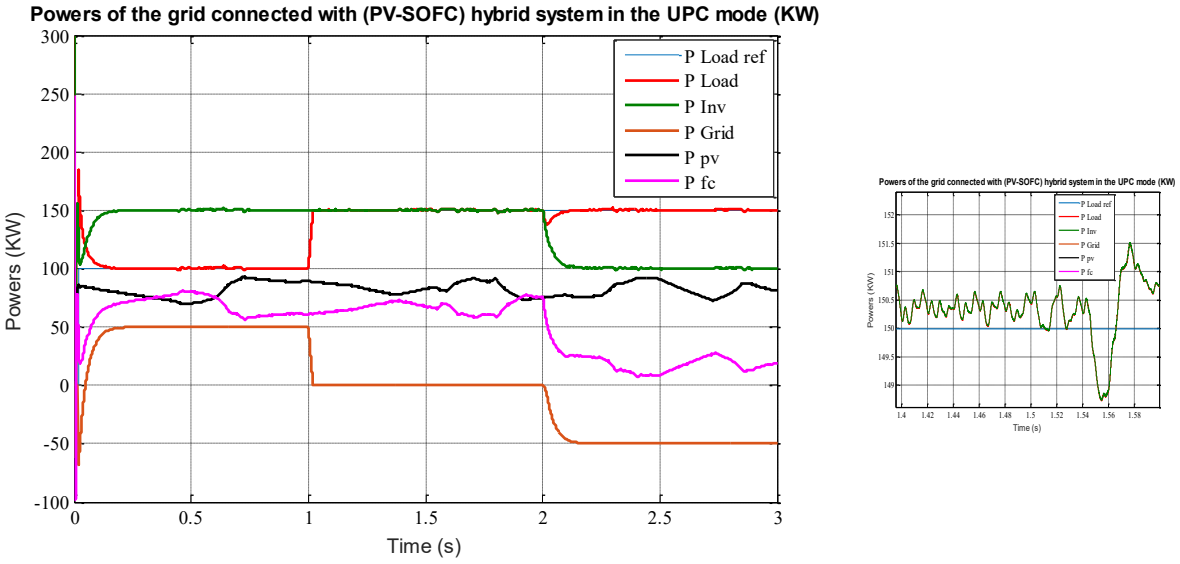

(a)

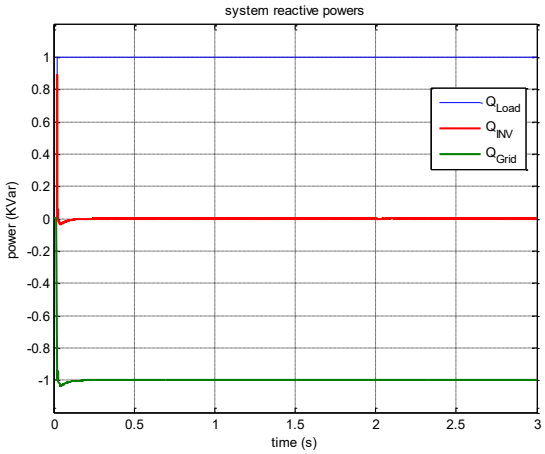

(b)

Figure 8. Grid-connected (PV-SOFC) system powers in the UPC mode under PSO-DISMC:

(a) active powers (with Zoom), (b) reactive powers

From the results, it can be seen that the output voltage and current of the SOFC depend on the PV array's output power (Fig. 6). In unfavorable atmospheric conditions, the SOFC increases its output to compensate for the drop in PV power production.

For : t<1s, (Fig. 8.a), even when the load power is *100 kW*, the system generates about *150 kW*. This achieves the objective of fixed UPC power. For : t>1s , due to the rising local load, the system maintains its production level, the primary grid supplies the remaining power needed by the load.

The reactive power reference is also controlled independently of the load. It is set to zero, and the system guarantees the grid reactive power (Q= -1Kvar in Fig. 8.b)

Each input capacitor of the three-level NPC inverter equals half of the DC bus voltage

(Fig. 7.a). Using SVPWM with PSO-DISMC further enhances the output AC voltage quality (THD = 3.13%) (Fig. 7.b).

The steady-state error between the NPC inverter's output power and the required power reference is nearly zero (see Fig. 8.a, zoomed view). This validates the controller's performance, despite some response delay from the SOFC time constant. The proposed control's robustness is further confirmed by its ability to handle capacitor voltage fluctuations and local AC load variations.

Conclusion

This work introduced a PSO-optimized discrete-time integral sliding mode control (DISMC) for a three-level NPC inverter, applied to the control and power management of a grid-connected PV-FC distributed power generation system. Simulation results for both Unit-Power Control (UPC) and Feeder-Flow Control (FFC) modes confirms that the PSO-DISMC achieves effective, decoupled transfer of active and reactive power between the PV, FC, local load, and the grid, while ensuring good quality of current and voltage. The proposed controller is formulated in the (*d, q*) frame, with discrete voltage references modulated by SVPWM. The use of the PSO technique enhances the stability and robustness of the sliding mode control as shown by better system performance under variable weather and load conditions, and improved transient response. DC voltage stability is maintained by localized control of each DC source.

REFERENCES

[1] Singhal, A., Vu, T. L., & Du, W. (2022). Consensus control for coordinating grid-forming and grid following inverters in microgrids. *IEEE Transactions on Smart Grid, 13*(5), 4123–4133. https://doi.org/10.1109/TSG.2022.3158254

[2] Khan, A. A., Minai, A. F., Pachauri, R. K., & Malik, H. (2022). Optimal sizing, control, and management strategies for hybrid renewable energy systems: A comprehensive review. Energies, 15(17), 6249. https://doi.org/10.3390/en15176249

[3] Shah, C., et al. (2021). Review of dynamic and transient modeling of power electronic converters for converter dominated power systems. *IEEE Access, 9*, 82094–82117. https://doi.org/10.1109/ACCESS.2021.3086420

[4] Andrew, L. D., & David, A. J. R. (2018). *Fuel cell systems explained* (1st ed.). John Wiley & Sons Ltd. https://doi.org/10.1002/9781118706992

[5] Trinadh, P., Cavus, M., Odigwe, I., Allahham, A., Walker, S., & Giaouris, D. (2023). A review of microgrid energy management strategies from the energy trilemma perspective. *Energies, 16*(1), 289. https://doi.org/10.3390/en16010289

[6] Lee, H. J., Choi, J. Y., Park, G. S., Oh, K. S., & Won, D. J. (2017). Renewable integration algorithm to compensate PV power using battery energy storage system. In *6th International Youth Conference on Energy* (pp. 1–6). IEEE. https://doi.org/10.1109/IYCE.2017.8003694

[7] Hazem, O. M., Amirat, Y., Benbouzid, M., & Elbaset, A. (2014). Optimal design of a PV/fuel cell hybrid power system for the city of Brest in France. In *IEEE ICGE* (pp. 119–123). https://doi.org/10.1109/ICGE.2014.6835408

[8] Tahir, S., Jie, W., Baloch, M. H., & Kaloi, G. S. (2018). Digital control techniques based on voltage source inverters in renewable energy applications: A review. *Electronics, 7*(2), 18. https://doi.org/10.3390/electronics7020018

[9] Lunardi, A., Normandia, L. F., Munkhchuluun, L. E., Meegahapola, L., & Filho, J. S. (2022). Grid-connected power converters: An overview of control strategies for renewable energy. *Energies, 15*(11), 4151. https://doi.org/10.3390/en15114151

[10] Utkin, V., Poznyak, A., Orlov, Y., & Polyakov, A. (2020). Conventional and high order sliding mode control. *Journal of the Franklin Institute, 357*(15), 10244–10261. https://doi.org/10.1016/j.jfranklin.2020.08.020

[11] Shtessel, Y., Edwards, C., Fridman, L., & Levant, A. (2016). *Sliding mode control and observation*. Control Engineering Series. Birkhäuser. https://doi.org/10.1007/978-0-8176-4893-0

[12] Villalva, M. G., Gazoli, J. R., & Filho, E. R. (2009). Comprehensive approach to modeling and simulation of photovoltaic arrays. *IEEE Transactions on Power Electronics, 24*(5), 1198–1208. https://doi.org/10.1109/TPEL.2009.2013862

[13] Chendong, Z., Mingfei, L., & Meilin, L. (2012). Chapter 2: Solid oxide fuel cells, sol-gel processing for conventional and alternative energy. In *Springer Science & Business Media* (pp. 7–36). https://doi.org/10.1007/978-1-4614-1957-0_2

[14] Channegowda, J., Saritha, B., Chola, H. R., & Narayanan, G. (2014). Comparative evaluation of switching and average models of a DC-DC boost converter for real-time simulation. In *IEEE International Conference on Electronics, Computing and Communication Technologies* (pp. 1–6). https://doi.org/10.1109/CONECCT.2014.6740360

[15] Putri, R. I., Wibowo, S., & Rifa'i, M. (2015). Maximum power point tracking for photovoltaic using incremental conductance method. *Energy Procedia, 68*, 22–30. https://doi.org/10.1016/j.egypro.2015.03.229

[16] Zeng, Z., Yang, H., Zhao, R., & Cheng, C. (2013). Topologies and control strategies of multi-functional grid-connected inverters for power quality enhancement: A comprehensive review.

Renewable and Sustainable Energy Reviews, 24, 223–270. https://doi.org/10.1016/j.rser.2013.03.033

[17] Sebaaly, F., Vahedi, H., Kanaan, H. Y., Moubayed, N., & Al-Haddad, K. (2016). Design and implementation of space vector modulation-based sliding mode control for grid-connected 3L-NPC inverter. *IEEE Transactions on Industrial Electronics, 63*(12), 7854–7863. https://doi.org/10.1109/TIE.2016.2582492

[18] Porru, M., Serpi, A., Marongiu, I., & Damiano, A. (2018). Suppression of DC-link voltage unbalance in three-level neutral-point clamped converters. *Journal of the Franklin Institute, 355*(2), 728–752. https://doi.org/10.1016/j.jfranklin.2017.11.039

[19] Venkatramanan, D., Johnson, B., & Dhople, S. (2021). Averaged dynamic model of three-level NPC grid-following inverter for examining neutral-point instability. In *IEEE 22nd Workshop on Control and Modelling of Power Electronics* (pp. 1–7). https://doi.org/10.1109/COMPEL52922.2021.9645941

[20] Abidi, K., & Xin, X. J. (2008). A discrete-time integral sliding mode control approach for output tracking with state estimation. *IFAC Proceedings Volumes, 41*(2), 14199–14204. https://doi.org/10.3182/20080706-5-KR-1001.02407

Research Article

[21] Yang, B., Sang, Y. Y., Shi, K., Yao, W., Jiang, L., & Yu, T. (2016). Design and real-time implementation of perturbation observer based sliding-mode control for VSC-HVDC systems. *Control Engineering Practice, 56*, 13–26. https://doi.org/10.1016/j.conengprac.2016.07.013

[22] Chai, C. H., & Osman, J. H. S. (2015). Discrete-time integral sliding mode control for large-scale system with unmatched uncertainty. *Journal of Control Engineering and Applied Informatics, 17*(3), 3–11. https://doi.org/10.1049/iet-cta.2008.0471

[23] Parsopoulos, K. E., & Vrahatis, M. N. (2010). *Practical swarm optimization and intelligence: Advances and applications*. Information Science Reference. https://doi.org/10.13140/2.1.3681.1206

[24] Radosavljevic, J. (2018). *Metaheuristic optimization in power engineering*. The Institution of Engineering and Technology. https://doi.org/10.1049/PBPO131E

Appendix

Parameters of the (SOFC) PI Controller : k_p =0.001, k_i=0.15

Parameters of the PSO-DISMC Controller :

- *mode FFC*

$$K_{PO} = \begin{bmatrix} 0.57 & 0 & 0 \\ 0 & 0.57 & 0 \\ 0 & 0 & 2.4 \end{bmatrix}, K_{IO} = \begin{bmatrix} 7.7 \cdot 10^3 & 0 & 0 \\ 0 & 7.7 \cdot 10^3 & 0 \\ 0 & 0 & 3.9 \cdot 10^3 \end{bmatrix}$$

- *mode UPC*

$$K_{PO} = \begin{bmatrix} 0.65 & 0 & 0 \\ 0 & 0.65 & 0 \\ 0 & 0 & 2.34 \end{bmatrix}, \quad K_{IO} = \begin{bmatrix} 7.9 \cdot 10^3 & 0 & 0 \\ 0 & 7.9 \cdot 10^3 & 0 \\ 0 & 0 & 3.2 \cdot 10^3 \end{bmatrix}$$

Table 1. Parameters of the Grid

Parameter	symbol	Value	Unit
Equivalent Input capacitor	C_{eq}	6.10^{-3}	F
Grid resistance and inductance	R_g L_g	0.012 6.10^{-4}	Ω , H

Table 2. Parameters of the (DC-DC) Boost converters

Parameter	***symbol***	***Value***	***Unit***
inductance	r_L , L	0.01 , 5.10^{-3}	Ω, H
Capacitor	r_C ,C	0.01 5.10^{-3}	Ω, F
Switching frequency	f_S	*5.4*	*Khz*

Table 3. Parameters of the three-level NPC Inverter

Parameter	symbol	Value	Unit
Rated power	$P_{inv\,n}$	2	kw
Output filter	L_f	4 .10-3	H
Switching frequency	f_S	5.4	Khz
Line-Line Voltage amplitude	$V_{L\text{-}L}$	400	VRms
Line-Neutral Voltage ampl	$V_{L\text{-}N}$	230	VRms

Journal of Information Systems Engineering and Management
2025, 10(4)
e-ISSN: 2468-4376
https://www.jisem-journal.com/

Research Article

Table 4. Parameters of the PV array (25°C)

Parameter	symbol	Value	Unit
Numbers of the series modules	Ns	5	
Numbers of the parallel modules	Np	66	
Numbers of the cells per module	n	96	
Open circuit voltage	Voc	64.2	V
Short-circuit current	Isc	5.96	A
Voltage at maximum power point	Vmp	54.7	V
Current at maximum power point	Imp	5.58	A
Photo-current	Iph	5.96	A
Diode saturation current Isat	Isat	5.26 .10-9	A
Parallel resistance	Rp	820	Ω
Series resistance	Rs	0.083	Ω

Table 5. Parameters of the SOFC

Parameter	symbol	Value	Unit
Standard reversible cell potential	E0	1.18	V
Number of cells in stack	N	450	
fuel ratio Max Min Optimum	Umax , Umin Uopt	0.9 , 0.8 , 0.85	
Value molar constant H2 , O2, H2O	KH2 KO2 KH2O	0.84 , 0.82, 2.52	mol/(s atm)
Response time H2 , O2, H2O	τH2 τO2 τH2O	26, 78, 2.5	s
Electric response time	Te	0.6	s
Fuel processor response time	Tf	0.03	s
Ratio of hydrogen to oxygen	rHO	1.145	
Ohmic loss	R	0.126	Ω
Faraday's constant	F	96487	C/mol
Universal gas constant	R	8314	J/ (Kmol K)